J. Mater. Environ. Sci. 7 (9) (2016) 3193-3210 *Elfaydy et al.*
ISSN : 2028-2508
CODEN: JMESC

Investigation of Corrosion Inhibition Mechanism of Quinoline Derivative on Mild Steel in 1.0 M HCl Solution: Experimental, Theoretical and Monte Carlo Simulation

M. Elfaydy[1], H. Lgaz[2,3], R. Salghi[3*], M. Larouj[2], S. Jodeh[4], M. Rbaa[1,2], H. Oudda[2], K. Toumiat[5], B. Lakhrissi[1]

[1]*Laboratoire d'Agroressources, Polymères et Génie des Procédés, University Ibn Tofail PO Box 242, Kenitra, Morocco.*
[2]*Laboratory separation processes, Faculty of Science, University Ibn Tofail PO Box 242, Kenitra, Morocco.*
[3]*Laboratory of Applied Chemistry and Environment, ENSA, Université Ibn Zohr,PO Box 1136, 80000 Agadir, Morocco*
[4]*Department of Chemistry, An-Najah National University, P. O. Box 7, Nablus, Palestine*
[5]*Department of Materials Sciences, Laghouat University, PO Box 37, 03000, Laghouat, Algeria*

Received 26 Feb 2016, Revised 18 Jul 2016, Accepted 24 Jul 2016
**Corresponding author. E-mail:* r.salghi@uiz.ac.ma *(R. Salghi); Phone: +212 6 61145512*

Abstract
The corrosion inhibition mechanism of 5-(((1H-benzimidazol-2-yl) thio) methyl) 8-quinolinol **(BTQ8)** on mild steel in 1.0 M HCl solution was investigated by weight loss, Tafel polarization and electrochemical impedance spectroscopy (EIS) techniques. The experimental results were supported by molecular dynamic simulation and DFT calculations. It was found that **BTQ8** acts by adsorption on mild steel via chemical interactions and a protective film formation. Tafel polarization method shows that **BTQ8** act as a mixed type inhibitor. The effect of temperature on the corrosion behavior of mild steel was studied in the range of 303–333 K. The results from this corrosion test clearly reveal that the inhibition efficiency (% IE) of **BTQ8** increased with increasing inhibitor concentration and decreased with increase in temperatures and the adsorption process of inhibitors obeyed the Langmuir isotherm. Theoretical calculations are in good agreement with the experiments results.

Keywords: Corrosion inhibition, quinoline, DFT, Molecular dynamic, mild steel, SEM

1. Introduction
Carbon steel is used in mass amounts in marine applications, chemical processing, petroleum production and refining, construction and metal-processing equipment [1–3]. Corrosion inhibitors are substances that when are added to an aggressive environment due to acid pickling, chemical cleaning and oil well acidification processes have the ability to reduce remarkably the rate of attack on the metals and alloys by decreasing the corrosion processes[4,5]. These organic molecules can be adsorbed on the metal surface because they are able to establish coordinative interactions between molecule atoms and the mild steel surface: as a result, the corrosive attack is reduced in acidic media [6–9].
The adsorption of organic molecules on metals surfaces depends mainly on the nature and the surface charge of metals, the chemical structure of organic molecule (functional groups, steric factors, electron density, etc.) and the type of solution[8–10]. The organic compounds having heteroatoms with high electron density such as sulfur, nitrogen, oxygen or those containing multiple bonds are effective inhibitors for the corrosion of metals[11–16].

The presence of such atoms with high electron density and multiple bonds in molecular structure enhance the adsorption ability of organic compounds.
In the recent times, the use of quantum chemical methods in the estimation of potential corrosion inhibitors has been extremely useful. Quantum chemical parameters which are based on the Density Functional Theory and molecular dynamic simulation have been the guide for investigating the agreement with experimental data of the results of computational chemistry works[17–19].
The quinolone derivatives are one of the important chemical compounds with variety applications[20–25]. Therefore, it is necessary to study the corrosion inhibition effect and inhibition mechanism of 5-(((1H-benzimidazol-2-yl) thio) methyl) 8-quinolinol **(BTQ8)** as new corrosion inhibitor.
In this investigation, electrochemical techniques, weight loss and scanning electron microscopy methods were employed to study the inhibition effect of 5-(((1H-benzimidazol-2-yl) thio) methyl) 8-quinolinol **(BTQ8)** for mild steel in 1.0 M HCl solution. And then, quantum chemical calculations by Molecular dynamic simulation and DFT method were performed to obtain more information about the interaction between the inhibitor molecules and mild steel surface.

2. Materials and methods

2.1. Synthesis of BTQ8

❖ **General Information**

All chemicals products were purchased from commercial suppliers Aldrich or Acros (France or Spain), and were used without further purification. ^{1}H and ^{13}C NMR spectra were recorded on a model Bruker Avance (300 MHz) for solutions in Me_2SO-d_6, and Chemical shifts are given as δ values with reference to tetramethylsilane (TMS) as internal standard. The progress of the reaction was followed by Thin-Layer Chromatography (TLC) using silica gel 60 F254 (E. Merck) plates with visualization by UV light (254 nm). Melting points were determined on an automatic electrothermal IA 9200 digital melting point apparatus in capillary tubes and are uncorrected.

❖ **Chemical synthesis**

Synthesis of 5-(((1H-benzimidazol-2-yl) thio) methyl) quinolin-8-ol

The preparation of 5-(((1H-benzimidazol-2-yl) thio) methyl) 8-quinolinol require at first the preparation of 2-mercaptobenzimidazole (1), which was *prepared* according to the literature method [24].

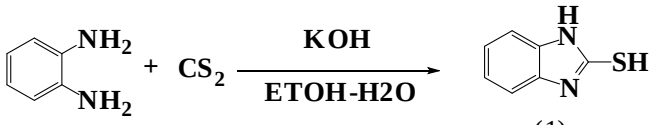

(R. 1)

(1)

Scheme 1: Synthetic scheme for the synthesis of 2-mercaptobenzimidazole (1)

On the other hand, 5-chloromethyl-8-quinoline hydrochloride (2) was prepared according to the method reported in the literature [25].

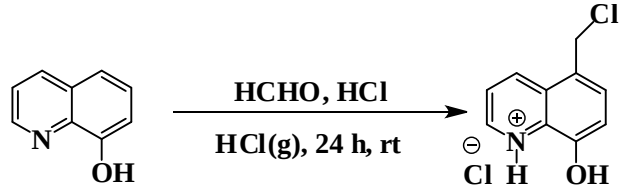

(R. 2)

(2)

Scheme 2: Synthetic scheme for the synthesis of 5-chloromethyl-8-quinoline hydrochloride (2)

The preparation of 5-(((1H-benzimidazol-2-yl) thio) methyl)-8-quinolinol is outlined in scheme 3,

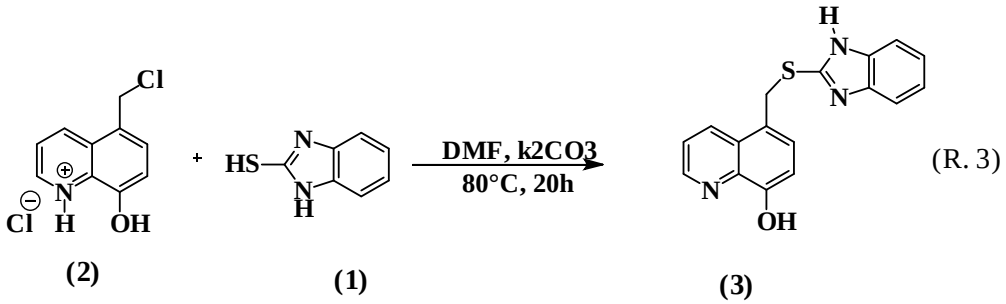

(R. 3)

Scheme 3: Synthesis of 5-(((1H-benzimidazol-2-yl) thio) methyl) 8-quinolinol

Synthesis of 5 -(((1H-benzimidazol-2-yl) thio) methyl)-8-quinolinol (3)

A mixture of chloromethyl-8-hydroxyquinoline hydrochloride (1 g, 0.00435 mol), benzimi-dazole-2-thiol (0.652 g, 0.00435 mol) and potassium carbonate (0.6 g, 0.00435 mol) in dimethylformamide (40 mL) was heated at 80 °C for 20 h. *After completing* the *reaction*, the resulting *mixture was poured* into 50 mL of cold water. The precipitate formed was separated from the solution by filtration, washed with water for several times and purified by recrystallizing from DMF-EtOH mixture to afford (**3**) as a white solid (0.96 g, 72 % yield). The formation of the product was confirmed by TLC using hexane: acetone (60:40, v/v) mixture as the mobile phase. Mp = 230-232 °C, ^{1}H NMR (300 MHz, DMSO-d_6), δ_{ppm} = 9.82-9.88 (s, 1 H, quinoline (C-OH)), 6.99-8.86 (m, 9 H, quinoline and benzene), 5.87 (s, 2 H, quinoline -CH_2-S), 12.98 (s, 1 H, NH of imidazol), 3.40 (s, H of trace H_2O present in DMSO-d_6), ^{13}C NMR (300 MHz, DMSO-d_6), δ_{ppm} = 36.26 (quinoline -CH_2 -S), 110.57, 110.88, 121.90, 122.43, 122.78, 123.49, 127.06, 127.43, 132.93, 132.97, 139.15, 148.56, 153.60, (CH. C quinoline, benzene and N=C-N).

^{1}H NMR spectra (300 MHz, Me_2SO-d_6)

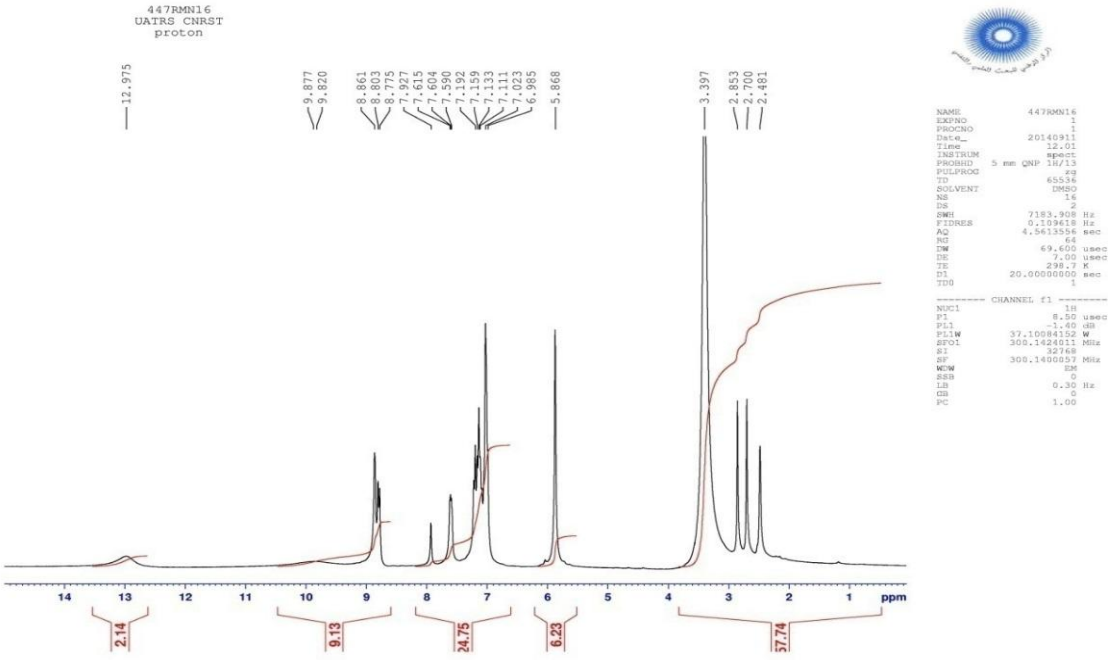

Figure 1: ^{1}H NMR spectrum of 5 -(((1H-benzimidazol-2-yl) thio) methyl)-8-quinolinol

^{13}C NMR spectra (300 MHz, Me_2SO-d_6)

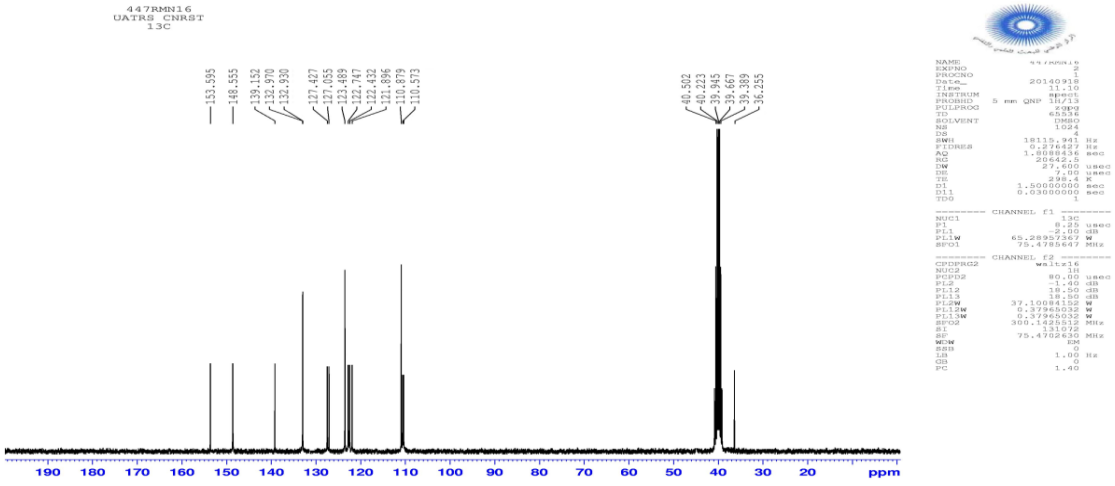

Figure 2: ^{13}C NMR spectrum of 5 -(((1H-benzimidazol-2-yl) thio) methyl)-8-quinolinol

2.2. Gravimetric, Electrochemical measurements and Electrolytic solution

The gravimetric measurements were carried out at definite time interval of 6 h using an analytical balance (precision ± 0.1 mg), The steel specimens of dimension 2x2x0.08 cm^3 used in this study is a carbon steel (Euronorm: C35E carbon steel and US specification: SAE 1035) with a chemical composition (in wt%) of 0.370% C, 0.230% Si, 0.680% Mn, 0.016% S, 0.077% Cr, 0.011% Ti, 0.059% Ni, 0.009% Co, 0.160% Cu and the remainder iron (Fe). The surface of the test electrode was mechanically abraded by different grades of emery papers with 220 up to 1500, washed with distilled water, cleaned with acetone after being weighed accurately with high sensitivity balance, the specimens were carried out in a double glass cell equipped with a thermostated cooling condenser containing 80 mL of non-de-aerated test solution with and without various concentrations of the studied quinoline derivative (**BTQ8)** at 303K, and at different temperatures (303 – 333K) for 10^{-3} M concentration. After immersion period, the specimens were taken out, rinsed thoroughly with bidistilled water, dried and weighed accurately again. Five tests were performed in each case and the mean value of the weight loss was calculated. The electrochemical experience have been performed using an equipment of impedance (Tacussel Radiometer PGZ 100), the data were analyzed using software VoltaMaster 4. A cell of Pyrex glass with three cylindrical electrodes has been used. To control temperature a thermostat has been used. A platinum auxiliary electrode and saturated calomel electrode (SCE) as reference electrode. The working electrode was carbon steel with the surface area of 1 cm $^{(2)}$. All potentials are reported vs. SCE. Prior to the electrochemical experiments, the mild steel was immersed into the test solution for 30min until a steady-state (open circuit) potential was obtained. EIS measurements were performed with a frequency range of 10 mHz to 100 kHz and amplitude of 5 mV with 10 points per decade. The polarization curves were recorded by polarization from -800 to -200 mV/SCE with a scan rate of 60 mV s−1. ZView software version 2.8 was used to fit impedance data. Acid solutions (1.0 M HCl) were prepared by diluting a reagent of analytical grade HCl 37% with double-distilled water. The concentration range of the quinoline derivative was used was 10^{-6} to 10^{-3} M.

2.3. Quantum chemical calculations

It should be stated that DFT methods are widely used in computational chemistry studies because these methods have become very popular in recent times [26,27]. Quantum chemical calculations were performed using density functional theory (DFT) with the Beck's three parameter exchange functional along with the Lee-Yang-Parr non local correlation functional (B3LYP) with 6-31G (d, p) basis set is implemented in Gaussian 03 program

package[28–33]. This approach is widely utilized in the analysis of the characteristics of corrosion process. The following quantum chemical parameters were evaluated from the optimized molecular structure: the dipole moment (μ), the energy of the highest occupied molecular orbital (E_{HOMO}), the energy of the lowest unoccupied molecular orbital (E_{LUMO}), the energy band gap ($\Delta Egap = E_{HOMO} - E_{LUMO}$), the electron affinity (A), the ionization potential (I) and the number of transferred electrons (ΔN).

2.4. Molecular dynamic simulation

The Monte Carlo (MC) search was adopted to compute the low configuration adsorption energy of the interactions of the **BTQ8** on a clean iron surface. The Monte Carlo (MC) simulation was carried out using Materials Studio 6.0 software (Accelrys, Inc.)[34]. The Fe crystal was cleaved along the (110) plane, it is the most stable surface as reported in the literature. Then, the Fe (110) plane was enlarged to (12×12) supercell to provide a large surface for the interaction of the inhibitor. The simulation of the interaction between **BTQ8** and the Fe (110) surface was carried out in a simulation box (29.78 × 29.78 × 60.13 Å) with periodic boundary conditions, which modeled a representative part of the interface devoid of any arbitrary boundary effects. After that, a vacuum slab with 50 Å thickness was built above the Fe (110) plane. All simulations were implemented with the COMPASS force field to optimize the structures of all components of the system of interest. More simulation details on the methodology of Monte Carlo simulations can be found in previous publications[35,36]

3. Results and discussion

3.1. Weight loss measurements

3.1.1 Effect of concentration

Weight loss measurements were performed in the absence and presence of different concentrations of **BTQ8** at 303 K. The values of inhibition efficiency and corrosion rate (C_R) are presented in Table 1 and Fig. 3. The inhibition efficiency (η_w (%)) is calculated by the following Eq. 1:

$$\eta_w(\%) = \frac{C_R - C_{R(inh)}}{C_R} x\ 100 \quad (1)$$

Where C_R and $C_{R(inh)}$ represent the corrosion rates in the absence and presence of **BTQ8**.

Table 1. Inhibition efficiencies of various concentrations of **BTQ8** for corrosion of mild steel in 1.0 M HCl obtained by weight loss measurement at 303K.

Inhibitors	Concentration (M)	C_R (mg cm^{-2} h^{-1})	η_w (%)	Θ
BLANK	1.0	1.135	-	-
BTQ8	10^{-3}	0.056	**95.07**	0.9507
	10^{-4}	0.083	92.69	0.9269
	10^{-5}	0.153	86.52	0.8652
	10^{-6}	0.202	82.20	0.8220

Inspection of the data in Table 1 and Fig. 3, reveals that the corrosion rates decreases significantly in the presence of the inhibitor and the inhibition efficiency of inhibitor increased with increasing concentration of inhibitor. The corrosion rates of mild steel in the blank solution was 1.135 mg/cm^2 h and the addition of 10^{-3} M of **BTQ8** seed husk reduced the dissolution to 0.056 mg/cm^2h. Such behavior can be interpreted on the basis that the inhibitor exert their action by adsorbing themselves on the mild steel[37,38].

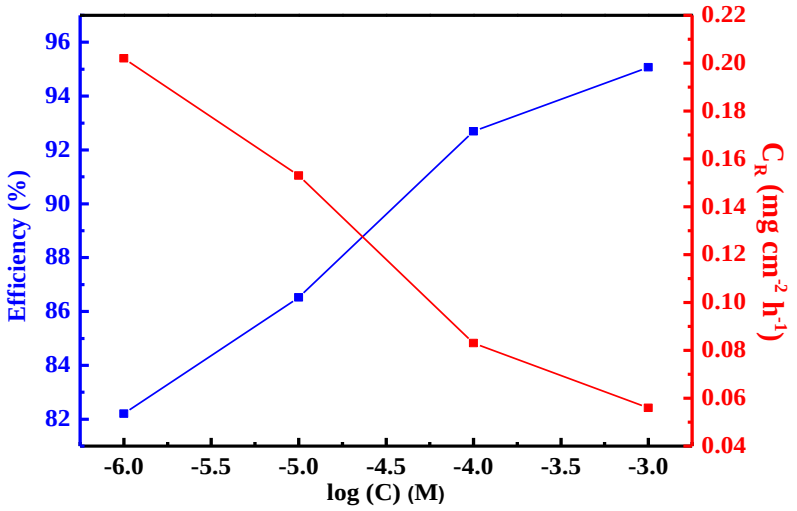

Figure 3 : Relationship between the inhibition efficiency and corrosion rates *vs. log*(C) for carbon steel after 6 h immersion in 1 M HCl at 303 K.

3.1.2. Effect of temperature

Generally speaking, the impact of temperature on the corrosion process of metal in aggressive solution is complex, because many changes occur on the metal/solution interface, such as rapid etching, desorption of inhibitors and the decomposition or rearrangement of inhibitor itself[39,40]. In order to study the effect of temperature on the inhibition performance of **BTQ8**, weight loss measurements was performed in 1.0 M HCl in the absence and presence of 10^{-3} M of inhibitor from 303 to 333 K. Results obtained after 6 h exposure time are presented in Table 2.

Table 2: C_R and η_w % obtained from weight loss measurements of mild steel in 1.0 M HCl containing 10^{-3} M of **BTQ8** at different temperatures.

Inhibitors	Temperature (K)	C_R (mg cm^{-2} h^{-1})	η_w (%)	Θ
Blank	303	1.135	-	-
	313	2.466	-	-
	323	5.032	-	-
	333	10.029	-	-
BTQ8	303	0.056	95.07	0.950
	313	0.256	89.62	0.896
	323	1.023	79.67	0.796
	333	3.512	64.98	0.649

The results obtained from Table 2, reveal that the corrosion rate increased with increase in temperature in both uninhibited and inhibited solution. Also the inhibition efficiency is observed to decrease with increase in temperature. The decrease in inhibition efficiency with temperature might be attributed to desorption of the inhibitor molecules from the metal surface at higher temperatures[41,42].

To calculate activation parameters of the corrosion process, Arrhenius Eq. (2) and transition state Eq. (3) were used[5,6]

$$C_R = k\ exp\left(\frac{-E_a}{RT}\right) \quad (2)$$

$$C_R = \frac{RT}{Nh}\ exp\left(\frac{\Delta S_a}{R}\right) exp\left(-\frac{\Delta H_a}{RT}\right) \quad (3)$$

where, Ea is the activation energy, ΔSa is the entropy of activation, ΔHa is the enthalpy of activation, *k* is the Arrhenius pre-exponential factor, *h* is Planck's constant, N is Avogadro's number, T is the absolute temperature and R is the universal gas constant.

Fig. 4 shows Arrhenius plots of logarithm of *ln* (CR) *vs* 1/T for mild steel in 1.0 M HCl without and with addition of 10^{-3} M of **BTQ8**. From the value of slope, the value of Ea were calculated for inhibitor and listed in Table 3. The value of Ea in the inhibited solution is higher than that for uninhibited solution, indicating that more energy barrier have been achieved in presence of **BTQ8** [43,44].

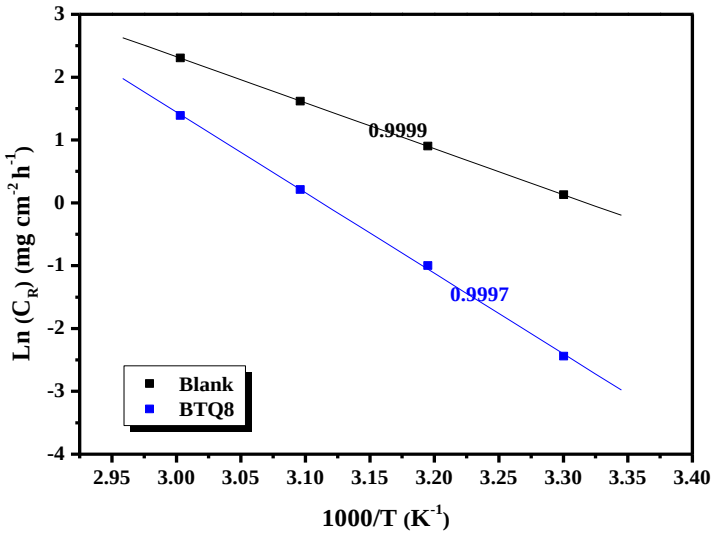

Figure 4: Arrhenius plots for mild steel in 1.0 M HCl in the absence and presence of 10^{-3} M of inhibitor at different temperatures.

Table 3: Activation parameters for mild steel corrosion in 1.0 M HCl in the absence and presence of 10^{-3} M of inhibitor at different temperatures.

Inhibitor	E_a (kJ/mol)	ΔH_a (kJ/mol)	ΔS_a (J mol-1 K-1)	E_a - ΔH_a
Blank	60.79	58.16	-51.84	2.63
10^{-3} M BTQ8	115.80	113.16	104.89	2.64

Using Eq. (3), another linear plot of ln C_R/T versus 1/T was drawn (Fig. 5) with slope (−ΔHa/R) and intercept [ln(R/Nh) + ΔSa/R] which was used for the calculation of ΔHa and ΔSa. All the values are listed in Table 3. The positive value of ΔHa reflect that the dissolution process of metal is endothermic[39,45]. ΔSa value is more

positive in presence of the studied inhibitor compared to HCl solution. The increase of ΔSa in the presence of inhibitor implies that the activated **BTQ8** in the rate determining step represent an association rather than a dissociation step[46,47].

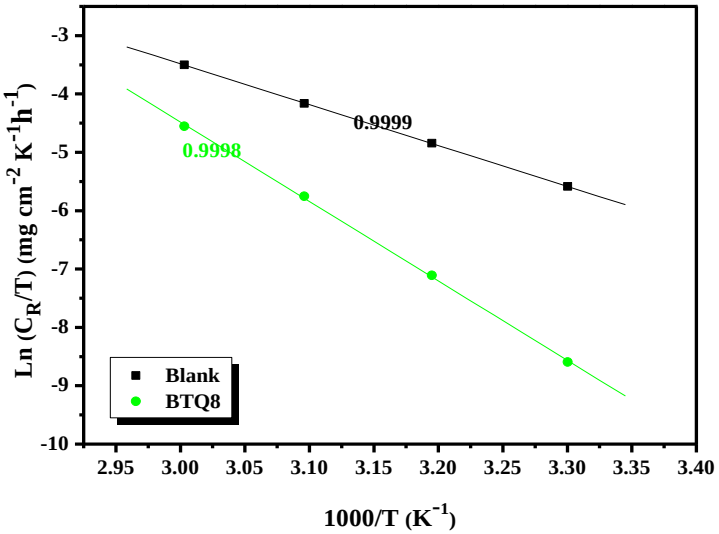

Figure 5: Transition state plots for the inhibition of corrosion of mild steel in 1.0 M HCl in the absence and presence of 10^{-3} M of inhibitor at different temperatures.

3.2. Adsorption Isotherm

Adsorption study was performed to understand the inhibiting effect of organic molecules on metal corrosion. It is accepted that inhibitor covers the iron surface by replacing the pre-adsorbed water molecules which act as a corrosive medium by the following equilibrium (Eq. 4)[48,49].

$$\mathrm{Org}_{(sol)} + \mathrm{xH_2O}_{(ads)} \rightarrow \mathrm{Org}_{(ads)} + \mathrm{xH_2O}_{(sol)} \quad (4)$$

where *x* is the number of H_2O molecules replaced by one organic molecule.

At present, adsorption isotherm can provide meaningful information about the interaction between additive and mild steel, based on the inference that the coverage of organic molecules is directly related to inhibition efficiency.

The degree of surface coverage (θ) obtained from potentiodynamic polarisation technique was used to evaluate the best isotherm that fits into the data obtained. Langmuir isotherm was applied to investigate whether it best fits to the experimental data obtained by using Eq. (5)[50,51].

$$\frac{C}{\theta} = \frac{1}{K_{ads}} + C \quad (5)$$

where C is the inhibitor concentration, θ is the surface coverage and K_{ads} is the adsorption equilibrium constant. The plot of C/θ versus C yields a straight line with a slope close to 1 (1.06) and the linear association coefficient (R^2) is also nearly 1 (0.9999), as shown in Fig. 6, indicating that the adsorption of **BTQ8** on the mild steel surface obeys Langmuir adsorption isotherm.

The standard free energy of adsorption ($\Delta G°_{ads}$) was calculated by using the following expression (Eq. 6) [52,53]

$$\Delta G°_{ads} = -RT \ln(55.5 \times K_{ads}) \quad (6)$$

where R is the universal gas constant, 55.5 is the concentration of water in solution and T (K) is the thermodynamic temperature. The calculated values of $\Delta G°_{ads}$ and K_{ads} for quinoline derivative listed in Table 4**.**

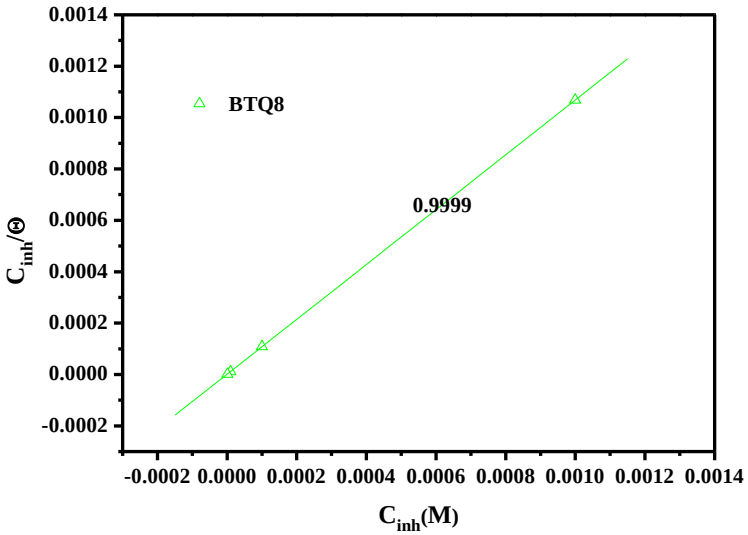

Figure 6: Langmuir adsorption of inhibitor on the carbon steel surface in 1.0 M HCl solution at 303K.

Table 4: Adsorption parameters of inhibitor for mild steel corrosion in 1M HCl at 303K

Inhibitor	Slope	$K_{ads}(M^{-1})$	ΔG°_{ads} (kJ/mol)
10^{-3} M **BTQ8**	1.06	975200.65	-44.84

The negative value of $\Delta G°_{ads}$ and the higher value of K_{ads} reveal the spontaneity of adsorption process and they are characteristic of strong interaction and stability of the adsorbed layer with the mild steel surface[54].
Generally, the energy values of −20 kJ mol^{-1} or less negative are associated with an electrostatic interaction between charged molecules and charged metal surface, physisorption; those of −40 kJ mol^{-1} or more negative involve charge sharing or transfer from the inhibitor molecules to the metal surface to form a coordinate covalent bond, chemisorption[55,56]. The value of $\Delta G°_{ads}$ listed in Table 4 indicate the chemisorption of quinoline derivative on the mild steel surface[57,58].

3.3. Potentiodynamic Polarization Studies

The potentiodynamic polarization curves for mild steel in 1 M HCl solution at 303 K containing various concentrations of **BTQ8** was studied by potentiodynamic polarization. Fig. 7 shows the polarization curves in the absence and presence of various concentrations of quinoline derivative. The electrochemical polarization parameters such as corrosion potential (E_{corr}), corrosion current density (i_{corr}), slope of the cathodic branch (βc), and corresponding percentage inhibition efficiencies (η_{PDP}%) were calculated and listed in Table 5. The values of η_{PDP} (%) were calculated using the following Eq. 7.

$$\eta_{PDP}(\%) = \frac{I_{corr} - I_{corr\ (i)}}{I_{corr}} \text{x } 100 \qquad (7)$$

Where I_{corr} and $I_{corr(i)}$ are the corrosion current densities for mild steel electrode in the uninhibited and inhibited solutions, respectively.

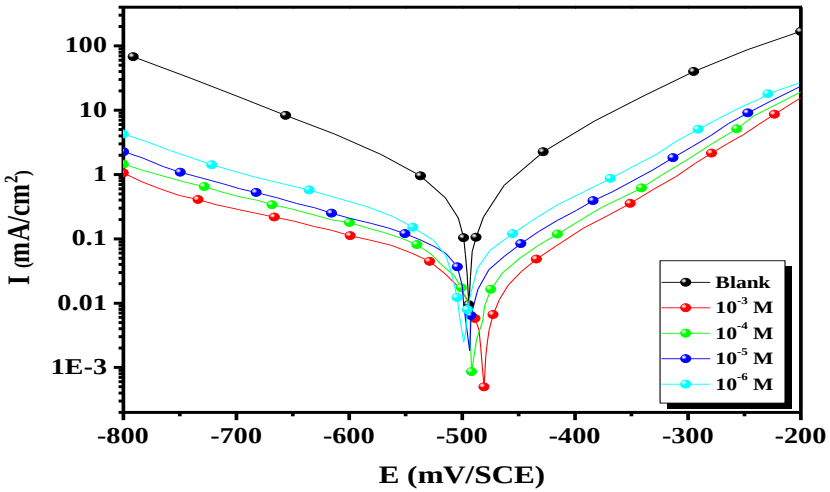

Figure 7: Polarisation curves of carbon steel in 1.0 M HCl for various concentrations of BTQ8 at 303K.

The addition of **BTQ8** decreased the corrosion current, I_{corr} significantly for all the concentrations studied, correspondingly, $\eta_{PDP}(\%)$ values increase with increasing the inhibitor concentration reaching a maximum value at 10^{-3} M of inhibitor. A compound can be regarded as a cathodic or anodic inhibitor in case the shifting in corrosion potential is over 85 mV with respect to that of the blank solution. In our study the potential shifts in the presence of **BTQ8** are less than 85 mV, showing that the inhibitor acts as a mixed-type inhibitor. Both the parallel Tafel curves in Fig. 7 and the almost unchanged values of slop in Table 5 indicate the corrosion reaction of metallic materials is kinetics-controlled and that the adsorbed inhibitor does not change the primary mechanism[17,59,60].

Table 5: Corrosion parameters for corrosion of mild steel with selected concentrations of the inhibitor in 1.0 M HCl by Potentiodynamic polarization method at 303K

Inhibitor	Concentration (M)	$-E_{corr}$ (mV/SCE)	$-\beta c$ (mV dec^{-1})	I_{corr} (µA cm^{-2})	$\eta_{PDP}(\%)$	Θ
BLANK	1.0	496	162.0	564.0	-	-
BTQ8	10^{-3}	480	185.2	35.9	93.63	0.936
	10^{-4}	491	185.1	46.8	91.70	0.917
	10^{-5}	494	163.7	66.1	88.28	0.882
	10^{-6}	498	165.2	127.8	77.34	0.773

3.4. Impedance Spectroscopic Studies

The inhibition performance of **BTQ8** for the acid corrosion of mild steel was evaluated by EIS. Fig. 8 shows the Nyquist plots in 1.0 M hydrochloric acid solution containing different concentrations of **BTQ8**. The irregular semicircles derived from impedance data indicate a non-ideal electrochemical behavior on the electrode surface, which may be due to frequency dispersion, inhomegeneties, roughness of metal surface and substance transmission actions[61,62]. As can be seen from Fig. 8, the Nyquist diagrams in the presence of **BTQ8** are similar to the blank one, this remark suggest that the inhibitor compound blocks the corrosion behavior of mild steel by controlling the activation of electrochemical reaction without changing its nature. In Fig. 8 we can only observe a capacitive loop which is related to the behavior of double layer capacitance as well as the charge

transfer process between metal surface and electrolyte[63,64]. The diameters of Nyquist plots increase as the concentration of **BTQ8** rises, suggesting the enhanced protection effect of inhibitor on the damage of metal in the corrosive solution[65].

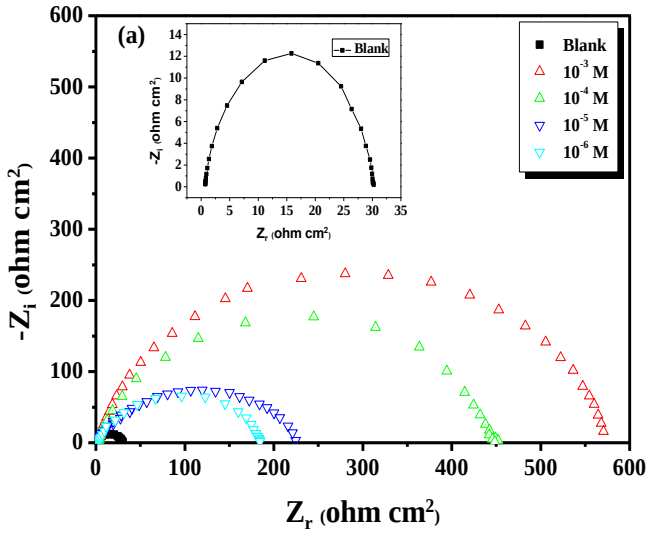

Figure 8: Nyquist curves for mild steel in 1M HCl for selected concentrations of **BTQ8** at 303K.

The experimental EIS data obtained are simulated by the proposed equivalent circuit presented in Fig. 10[66,67]. It included (Rs), the solution resistance, R_{ct} denotes the charge-transfer resistance and CPE is constant phase element. The introduction of CPE into the circuit was necessitated to explain the depression of the capacitance semicircle, which corresponds to surface heterogeneity resulting from surface roughness, impurities, and adsorption of inhibitor. The representative example of using the equivalent circuit to fit the experimental data for mild steel in 1.0 M HCl with 10^{-3} M of **BTQ8** is shown in Fig. 9 and the electrochemical parameters are listed in Table 6. From results obtained, R_{ct} increase with increase in inhibitor concentrations. Suggesting the formation of an isolating protective film at the metal/solution interface[68]. The impedance parameters obtained are reported in Table 6. The CPE impedance is calculated using the Eq. (8)

$$Z_{CPE} = \frac{1}{Q\,(j\omega)^n} \qquad (8)$$

Where *Q* is the *CPE* constant (in Ω^{-1} S^n cm^{-2}), ω is the angular frequency (in rad s^{-1}), j^2 = -1 is the imaginary number and *n* is a CPE exponent which can be used as a gauge for the heterogeneity or roughness of the surface. In addition, the double layer capacitances, C_{dl}, for a circuit including a *CPE* were calculated by using the following Eq. 9 [68]:

$$C_{dl} = (Q.R_{ct}^{1-n})^{1/n} \qquad (9)$$

The inhibition efficiency is calculated from the R_{ct} values using the following Eq. 10:

$$\eta_{EIS} = \frac{R_{ct} - R^{\circ}_{ct}}{R_{ct}} x\ 100 \qquad (10)$$

Where $R°_{ct}$ and R_{ct} are the charge transfer resistances without and with various concentrations of inhibitor respectively.

Table 6: AC-impedance parameters for corrosion of mild steel for selected concentrations of the inhibitor in 1 M HCl at 303K.

Inhibitor	Conc (M)	R_{ct} ($\Omega\ cm^2$)	n	$Q\times10^{-4}$ ($s^n\ \Omega^{-1}cm^{-2}$)	C_{dl} ($\mu F\ cm^{-2}$)	η_{EIS} (%)	Θ
Blank	1.0	29 .35	0.910	1.7610	91.6	-	-
BTQ8	10^{-3}	566.4	0.903	0.2065	12.8	**94.82**	0.948
	10^{-4}	446.5	0.897	0.2934	17.8	93.42	0.934
	10^{-5}	234.9	0.914	0. 3701	23.7	87.51	0.875
	10^{-6}	184.3	0.908	0.5122	31.9	84.07	0.840

The *IE* (%) values are high for the studied inhibitor indicating that they are good corrosion inhibition for mild steel in 1 M HCl. The calculated C_{dl} values in the presence of inhibitor are generally lower than that in solution without inhibitor. This implies that the inhibitor form protective film on the steel surface. The C_{dl} values also decrease with increasing concentration, this implies that the thickness of the protective film increases with increasing inhibitor concentration[69]. According to Helmholtz model (Eq. 11), the better inhibitive performance of the inhibitors is associated with lower *Q* value.

$$Q = \frac{\varepsilon^{\circ}\varepsilon}{d}A \qquad (11)$$

Where ε is the local dielectric constant, ε^0 is the permittivity of the air, d is the thickness of the protective layer and A is the surface area of the electrode. The decrease in Q suggests a fading in local dielectric constant or an increase in the thickness of the electrical double layer, due to the adsorption of quinoline derivative molecule on the mild steel surface by replacement of water molecules by quinoline derivative molecule[70,71].

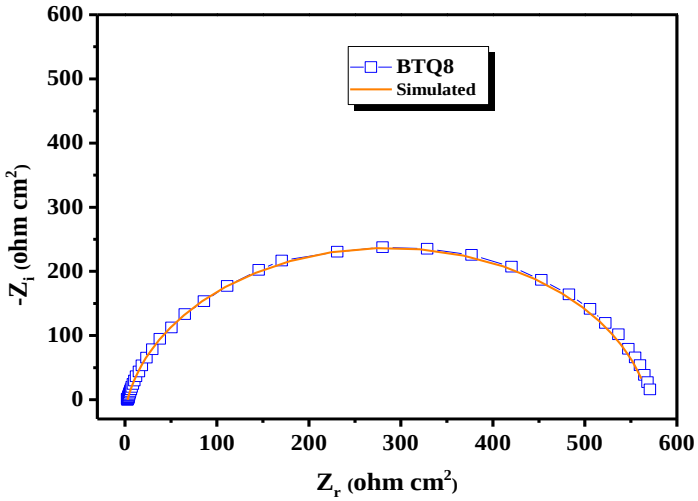

Figure 9: EIS Nyquist plots for carbon steel in 1 M HCl with 10^{-3}M of **BTQ8** interface: dotted lines experimental data; dashed line calculated.

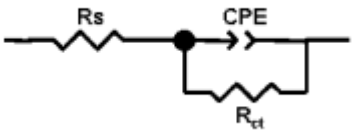

Figure 10: Equivalent electrical circuit corresponding to the corrosion process on the carbon steel in hydrochloric acid.

3.5. Quantum chemical calculation

3.5.1. DFT calculations

In our work, quantum chemical calculations were performed to obtain some details of molecular orbital which is a powerful theoretical tool to evaluate corrosion inhibitors. Two important frontier orbital parameters, the highest occupied molecular orbital (HOMO) and the lowest unoccupied molecular orbital (LUMO) represent the outmost and innermost orbital, respectively [17,18]. Generally speaking, the HOMO with rich charge functions as an electron donor since it tends to lose electrons. Accordingly the LUMO acts as an electron acceptor since it has empty orbitals to accept electrons. Fig. 12 illustrates the molecular orbital distribution of **BTQ8** molecule with optimized geometrical configuration. It can be seen from Fig. 11 that the distribution of HOMO and LUMO is localized on the entire molecule [19]. It is interesting to note that the LUMO distribution of **BTQ8** is mainly concentrated in the 8-hydroxyquinoline. This information reveals that this function may perform well in accepting electrons from the mild steel. Table 7 present the parameters obtained by DFT calculation, in density functional theory the energy of HOMO (E_{HOMO}) is regarded as the ionization potential and the higher magnitude indicates the better ability of molecules to provide metal electrons. On the other hand, the energy of LUMO (E_{LUMO}) is closely correlative with the electron affinity and the lower value suggests the easier transfer of electrons from metal surface to inhibitor. The energy gap between HOMO and LUMO (ΔE) represents the stability of transition complex which determines the interaction between the adsorbed inhibitor and the metallic substrate [30,33,72].

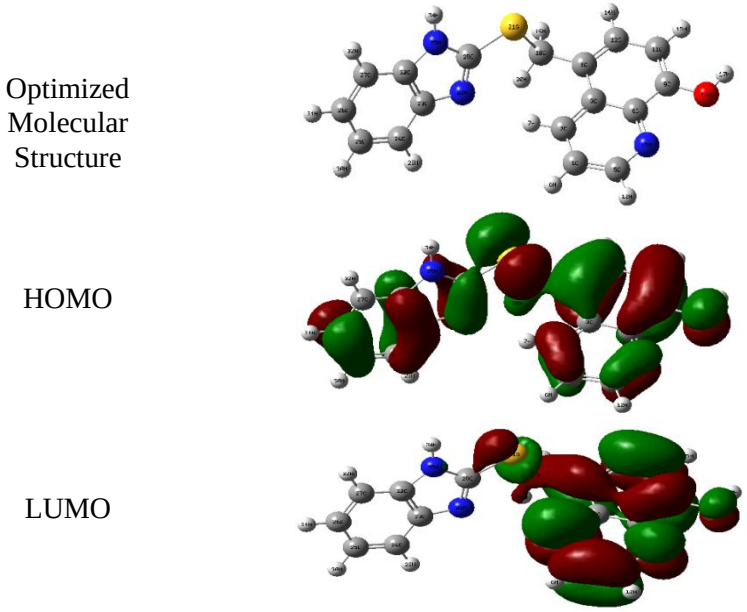

Figure 11: Quantum chemical results of BTQ8, calculated at DFT/B3LYB/6-31G (d, p)

For the dipole moment (μ), inhibitor with high dipole moment tend to form strong dipole–dipole interactions with the metal, resulting in strong adsorption on the surface of the metal and therefore leading to greater inhibition efficiency[74,75]. According to the hard–soft acid base (HSAB) principle, a hard molecule is associated with low basicity and low electron donating ability and a soft molecule is associated with high basicity and high electron donating tendency[76,77]. This finding suggests that the inhibition efficiency increases with increasing softness and decreases on increasing the hardness of the inhibitor molecules. Absolute electronegativity (χ), global hardness (η) and global softness (σ) are estimated using the equations (Eqs. 13-15)[65,78]

$$\chi = \frac{I + A}{2} \quad (12)$$

$$\eta = \frac{I - A}{2} \quad (13)$$

$$\sigma = \frac{1}{\eta} \quad (14)$$

The ionization potential (I) and the electron affinity (A) are defined as follows Eqs. 16-17:

$$I = -E_{HOMO} \quad (15)$$

$$A = -E_{LUMO} \quad (16)$$

The number of transferred electrons (ΔN) gives information about the number of electrons a molecule can transfer to the acceptor molecule, and it is estimated using the Eq. 18 [18,27]

$$\Delta N = \frac{\chi_{Fe} - \chi_{inh}}{2(\eta_{Fe} + \eta_{inh})} \quad (17)$$

where χ_{Fe} and χ_{inh} denote the absolute electronegativity of iron and the inhibitor molecule, respectively, and η_{Fe} and η_{inh} denote the absolute hardness of iron and the inhibitor molecule, respectively. The values of χ_{Fe} and η_{Fe} are taken as 7 eV mol^{-1} and 0 eV mol^{-1}, respectively. The results, as reported in Table 7, show the high number of electron transfer, which also confirms that **BTQ8** has the highest inhibition performance.

3.5.2. Molecular dynamic simulation

Adsorption of **BTQ8** molecules has been studied using molecular dynamics simulation techniques. Adsorption of **BTQ8** on iron substrate, Fe (110) has been studied to find the lowest energy adsorption sites on **BTQ8** molecules [36]. The best adsorption configuration for the compounds are presented in Fig. 12. From this figure, we can conclude that the studied compounds can be adsorbed on the Fe surface through the heteroatoms. A typical plot of energy distribution for inhibitor/Fe (110) system during energy optimization process consisting of the total energy, average total energy, van der Waals energy, electrostatic energy and intramolecular energy are presented in Fig. 13.

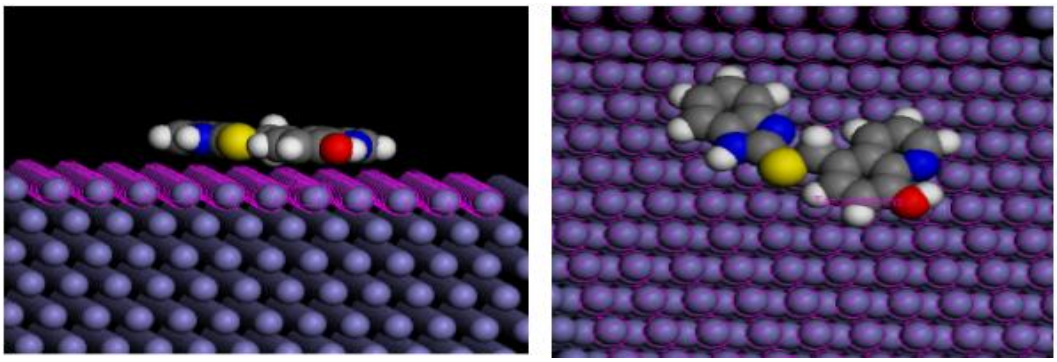

Figure 12: Side and top views of the most stable low energy configuration for the adsorption of the inhibitor on Fe (1 1 0) surface obtained through the Monte Carlo simulation of **BTQ8**.

The parameters presented in Table 8 include, the total energy, in kJ mol^{-1}, of the substrate–adsorbate configuration. The total energy is defined as the sum of the energies of the adsorbate components, the rigid adsorption energy and the deformation energy, adsorption energy reports the energy released (or required) when the relaxed adsorbate component was adsorbed on the substrate. The adsorption energy is defined as the sum of the rigid adsorption energy and the deformation energy for the adsorbate component. The rigid adsorption energy reports the energy released (or required) when the unrelaxed adsorbate component (before the geometry optimization step) was adsorbed on the substrate. The deformation energy reports the energy released when the adsorbed adsorbate component was relaxed on the substrate surface. Finally, (dEad/dNi) reports the energy of substrate–adsorbate configurations where one of the adsorbate components has been removed [87-88]. Further, results show that the high negative value of adsorption energy for investigated compounds, suggesting the better inhibition performance.

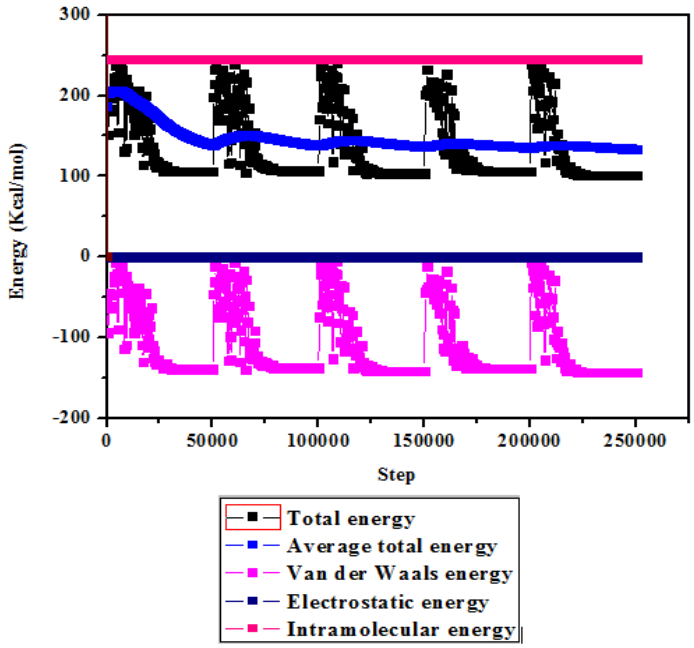

Figure 13: A typical energy profile for the adsorption progress of **BTQ8** on Fe (110) surface using the Monte Carlo sampling procedure.

Table 8: Outputs and descriptors calculated by the Monte Carlo simulation for the lowest adsorption. Configurations of **BTQ8**/Fe (110) surface (in kcal/mol).

System	Total energy	Adsorption energy	Rigid adsorption energy	Deformation energy	dEad/dNi inhibitor
Fe (1 1 0)/ **BTQ8**	23.02	-222.06	-246.26	24.2	-222.06

Conclusion

The study of **BTQ8** as a new and effective corrosion inhibitor of mild steel in 1 M HCl solution was conducted using weight loss, EIS, PDP measurements and theoretical calculations. From the results obtained herein, the following points were concluded:

- **BTQ8** acted as efficient corrosion inhibitor for mild steel in 1 M HCl solution.
- In the presence of inhibitor, charge transfer resistance (R_{ct}) increases and double layer capacitance (C_{dl}) decreases due to adsorption of the inhibitor molecules on the surface of mild steel.
- Polarization studies showed that the studied inhibitor act as mixed inhibitor.
- SEM analyses clearly show that **BTQ8** form a protective film on mild steel surface.
- The adsorption of the inhibitor on mild steel surface obeys the Langmuir adsorption isotherm. The negative sign of ΔG^0_{ads} suggests that the inhibitor adsorbed spontaneously on the surface.
- The Quantum chemical calculations by DFT calculations and Monte Carlo simulation are in good agreement with the experimental results.

References

1. Nwosu F.O., Muzakir M.M., J. Mater. Environ. Sci. 7 (2016) 1663–1673.

2. Larouj M., Lgaz H., Houda S., Zarrok H., Bourazmi H., Zarrouk A., Elmidaoui A., Guenbour A., Boukhris S., Oudda H., *J. Mater. Environ. Sci.* (2015) 3251–3267.
3. Afia L., Salghi R., Bammou L., Bazzi E., Hammouti B., Bazzi L., Bouyanzer A., *J. Saudi Chem. Soc*. 18 (2014) 19–25. doi:10.1016/j.jscs.2011.05.008.
4. Nahlé A., Abu-Abdoun I., Abdel-Rahman I., *J. Mater. Environ. Sci.* 7 (2016) 2955–2964.
5. Andreani S., Znini M., Paolini J., Majidi L., Hammouti B., Costa J., Muselli A., *J. Mater. Environ. Sci.* 7 (2016) 187–195.
6. Afia L., Salghi R., Bazzi E.H., Zarrouk A., Hammouti B., Bouri M., Zarrouk H., Bazzi L., Bammou L., *Res. Chem. Intermed.* 38 (2012) 1707–1717.
7. Hmamou D.B., Salghi R., Zarrouk A., Benali O., Fadel F., Zarrok H., Hammouti B., *Int. J. Ind. Chem.* 3 (2012) 1–9.
8. Afia L., Salghi R., Zarrouk A., Zarrok H., Bazzi E.H., Hammouti B., Zougagh M., *Trans. Indian Inst. Met.* 66 (2013) 43–49.
9. Hachelef H., Benmoussat A., Khelifa A., Athmani D., Bouchareb D., J. Mater. Environ. Sci. 7 (2016) 1751–1758.
10. Addi E.H.A., Bazzi L., Hilali M., Zine E.A., Salghi R., Issami S.E., *Can. J. Chem.* 81 (2003) 297–306.
11. Bousskri A., Anejjar A., Messali M., Salghi R., Benali O., Karzazi Y., Jodeh S., Zougagh M., Ebenso E.E., Hammouti B., *J. Mol. Liq.* 211 (2015) 1000–1008.
12. Hjouji M.Y., Djedid M., Elmsellem H., Rodi Y.K., Ouzidan Y., Chahdi F.O., Sebbar N.K., Essassi E.M., Abdel-Rahman I., Hammouti B., J. Mater. Environ. Sci. 7 (2016) 1425–1435.
13. Bammou L., Belkhaouda M., Salghi R., Benali O., Zarrouk A., Zarrok H., Hammouti B., *J. Assoc. Arab Univ. Basic Appl. Sci.* 16 (2014) 83–90.
14. Salghi R., Bazzi L., Hammouti B., Kertit S., Bouchtart A., El Alami Z., *Ann. Chim. Sci. Matér.* 25 (2000) 593–600.
15. Salghi R., Bazzi L., Zaafrani M., *Acta Chim. Slov*. 50 (2003) 491–504.
16. Salghi R., Mihit M., Hammouti B., Bazzi L., *J Iran ChemRes*. 2 (2009) 157–162.
17. Singh R.N., Kumar A., Tiwari R.K., Rawat P., *Acta. A. Mol. Biomol. Spectrosc.* 112 (2013) 182–190.
18. Jafari H., Danaee I., Eskandari H., RashvandAvei M., *J. Mater. Sci. Technol.* 30 (2014) 239–252.
19. Rodríguez-Valdez L.M., Villamisar W., Casales M., González-Rodriguez J.G., Martínez-Villafañe A., Martinez L., Glossman-Mitnik D., *Corros. Sci.* 48 (2006) 4053–4064.
20. Schimmer A.D., Jitkova Y., Gronda M., Wang Z., Brandwein J., Chen C., Gupta V., Schuh A., Yee K., Chen J., Ackloo S., Booth T., Keays S., Minden M.D., *Clin. LymphomaMyelomaLeuk.* 12 (2012) 330–336.
21. Daniel K.G., Chen D., Orlu S., Cui Q.C., Miller F.R., Dou Q.P., *Breast Cancer Res.* 7 (2005) R897.
22. Chen D., Cui Q.C., Yang H., Barrea R.A., Sarkar F.H., Sheng S., Yan B., Reddy G.P.V., Dou Q.P., *Cancer Res.* 67 (2007) 1636–1644.
23. Mao X., Li X., Sprangers R., Wang X., Venugopal A., Wood T., Zhang Y., Kuntz D.A., Coe E., Trudel S., Rose D., Batey R.A., Kay L.E., Schimmer A.D., *Leukemia*. 23 (2008) 585–590.
24. Choi B.Y., Jang B.G., Kim J.H., Seo J.-N., Wu G., Sohn M., Chung T.N., Suh S.W., *Neurobiol. Dis*. 54 (2013) 382–391.
25. Darby C.M., Nathan C.F., *J. Antimicrob. Chemother.* 65 (2010) 1424–1427. doi:10.1093/jac/dkq145.
26. Daoud D., Douadi T., Hamani H., Chafaa S., Al-Noaimi M., *Corros. Sci*. 94 (2015) 21–37.
27. Obot I.B., Macdonald D.D., Gasem Z.M., *Corros. Sci.* 99 (2015) 1–30.
28. Lukovits I., Kalman E., Zucchi F., *Corrosion*. 57 (2001) 3–8.
29. Parr R.G., Yang W., *J. Am. Chem. Soc*. 106 (1984) 4049–4050.
30. Lee C., Yang W., Parr R.G., *Phys. Rev. B.* 37 (1988) 785–789.
31. Parr R.G., Szentpaly L., Liu S., *J. Am. Chem. Soc*. 121 (1999) 1922–1924.
32. Li X., Deng S., Xie X., *J. Taiwan Inst. Chem. Eng.* 45 (2014) 1865–1875.

33. Frisch M. J., Trucks G. W., Schlegel H. B., Scuseria G. E., Robb M. A., Cheeseman J. R., Montgomery J. A., Vreven Jr., T., Kudin K. N., Burant J. C., Millam J. M., Iyengar S. S., Tomasi J., Barone V., Mennucci B., Cossi M., Scalmani G., Rega N., Petersson G. A., Nakatsuji H., Hada M., Ehara M., Toyota K., Fukuda R., Hasegawa J., Ishida M., Nakajima T., Honda Y., Kitao O., Nakai H., Klene M., Li X., Knox J. E., Hratchian H. P., Cross J. B., Bakken V., Adamo C., Jaramillo J., Gomperts R., Stratmann R. E., Yazyev O., Austin A. J., Cammi R., Pomelli C., Ochterski J. W., Ayala P. Y., Morokuma K., Voth G. A., Salvador P., Dannenberg J. J., Zakrzewski V. G., Dapprich S., Daniels A. D., Strain M. C., Farkas O., Malick D. K., Rabuck A. D., Raghavachari K., Foresman J. B., Ortiz J. V., Cui Q., Baboul A. G., Clifford S., Cioslowski J., Stefanov B. B., Liu G., Liashenko A., Piskorz P., Komaromi I., Martin R. L., Fox D. J., Keith T., Al-Laham M. A., Peng C. Y., Nanayakkara A., Challacombe M., Gill P. M. W., Johnson B., Chen W., Wong M. W., Gonzalez C., and Pople J. A., Gaussian 03, Revision C.02.
34. Materials Studio, Revision 6.0, Accelrys Inc., San Diego, USA, 2013.
35. Kaya S., Tüzün B., Kaya C., Obot I.B., *J. Taiwan Inst. Chem. Eng.* 58 (2016) 528–535.
36. Khaled K.F., El-Maghraby A., *Arab. J. Chem*. 7 (2014) 319–326.
37. Bazzi L., Salghi R., Zine E., Issami S.E., Kertit S., Hammouti B., *Can. J. Chem.* 80 (2002) 106–112.
38. Hmamou D.B., Salghi R., Zarrouk A., Zarrok H., Benali O., Errami M., Hammouti B., *Res. Chem. Intermed*. 39 (2013) 3291–3302.
39. Yüce A.O., Kardaş G., *Corros. Sci.* 58 (2012) 86–94.
40. Keleş H., Keleş M., Dehri İ., Serindağ O., *Colloids Surf. Physicochem. Eng. Asp.* 320 (2008) 138–145.
41. Mihit M., El Issami S., Bouklah M., Bazzi L., Hammouti B., Ait Addi E., Salghi R., Kertit S., *Appl. Surf. Sci*. 252 (2006) 2389–2395.
42. Mihit M., Laarej K., Abou El Makarim H., Bazzi L., Salghi R., Hammouti B., *Arab. J. Chem*. 3 (2010) 55–60.
43. Bahrami M.J., Hosseini S.M.A., Pilvar P., *Corros. Sci*. 52 (2010) 2793–2803.
44. Lebrini M., Bentiss F., Vezin H., Lagrenée M., *Corros. Sci.* 48 (2006) 1279–1291.
45. Daoud D., Douadi T., Issaadi S., Chafaa S., *Corros. Sci*. 79 (2014) 50–58.
46. Lebrini M., Robert F., Vezin H., Roos C., *Corros. Sci.* 52 (2010) 3367–3376.
47. Yıldız R., Doğan T., Dehrİ.,*Corros. Sci.* 85 (2014) 215–221.
48. Moretti G., Guidi F., Fabris F., *Corros. Sci.* 76 (2013) 206–218.
49. Kharchouf S., Majidi L., Bouklah M., Hammouti B., Bouyanzer A., Aouniti A., *Arab. J. Chem*. 7 (2014) 680–686.
50. Solmaz R., *Corros. Sci*. 81 (2014) 75–84.
51. Solmaz R., AltunbaşŞahin E., Döner A., Kardaş G., *Corros. Sci*. 53 (2011) 3231–3240.
52. Negm N.A., Elkholy Y.M., Zahran M.K., Tawfik S.M., *Corros. Sci*. 52 (2010) 3523–3536.
53. Amin M.A., Ibrahim M.M., *Corros. Sci*. 53 (2011) 873–885. doi:10.1016/j.corsci.2010.10.022.
54. Keleş H., Keleş M., Dehri İ., Serindağ O., *Colloids Surf. Physicochem. Eng. Asp*. 320 (2008) 138–145.
55. Kharchouf S., Majidi L., Bouklah M., Hammouti B., Bouyanzer A., Aouniti A., *Arab. J. Chem*. 7 (2014) 680–686.
56. Lebrini M., Robert F., Vezin H., Roos C., *Corros. Sci.* 52 (2010) 3367–3376.
57. Abiola O., Oforka N., *Mater. Chem. Phys.* 83 (2004) 315–322.
58. Wang X., Yang H., Wang F., *Corros. Sci*. 53 (2011) 113–121.
59. Verma C., Quraishi M.A., A. *J. Mol. Liq*. 212 (2015) 804–812.
60. Verma C., Ebenso E.E., Bahadur I., Obot I.B., Quraishi M.A., *J. Mol. Liq.* 212 (2015) 209–218.
61. Daoud D., Douadi T., Issaadi S., Chafaa S., *Corros. Sci*. 79 (2014) 50–58.
62. Ahamad I., Prasad R., Quraishi M.A., *Corros. Sci.* 52 (2010) 933–942.
63. Singh P., Singh A., Quraishi M.A., *J. Taiwan Inst. Chem. Eng*. doi:10.1016/j.jtice.2015.10.033.
64. Odewunmi N.A., Umoren S.A., Gasem Z.M., *J. Environ. Chem. Eng.* 3 (2015) 286–296.
65. Eddy N.O., Momoh-Yahaya H., Oguzie E.E., *J. Adv. Res*. 6 (2015) 203–217.

66. Zhang D., Tang Y., Qi S., Dong D., Cang H., Lu G., *Corros. Sci*. 102 (2016) 517–522.
67. Hussin M.H., Rahim A.A., Mohamad Ibrahim M.N., Brosse N., *Measurement*, 78 (2016) 90–103.
68. Khaled K.F., *ElectrochimicaActa*. 55 (2010) 6523–6532.
69. Muthukrishnan P., Prakash P., Jeyaprabha B., Shankar K., *Arab. J. Chem*. doi:10.1016/j.arabjc.2015.09.005.
70. Gupta N.K., Verma C., Quraishi M.A., Mukherjee A.K., *J. Mol. Liq*. 215 (2016) 47–57.
71. Ansari K.R., Quraishi M.A., Singh A., *Corros. Sci*. 79 (2014) 5–15.
72. Becke A.D., *Phys. Rev. A*. 38 (1988) 3098–3100.
73. Wazzan N.A., *J. Ind. Eng. Chem*. 26 (2015) 291–308.
74. Danaee I., Ghasemi O., Rashed G.R., RashvandAvei M., Maddahy M.H., *J. Mol. Struct*. 1035 (2013) 247–259.
75. Ramya K., Mohan R., Anupama K.K., Joseph A., *Mater. Chem. Phys*. 149–150 (2015) 632–647.
76. Obot I.B., Gasem Z.M., *Corros. Sci*. 83 (2014) 359–366.
77. Guo L., Ren X., Zhou Y., Xu S., Gong Y., Zhang S., *Arab. J. Chem*. doi:10.1016/j.arabjc.2015.01.005.
78. Olasunkanmi L.O., Kabanda M.M., Ebenso E.E., *Phys. E Low-Dimens. Syst. Nanostructures.* 76 (2016) 109–126.